# Characterization of wurtzite ZnO using valence electron energy loss spectroscopy

Michael R. S. Huang,[1] Rolf Erni,[2] Hsin-Ying Lin,[1] Ruey-Chi Wang,[3] and Chuan-Pu Liu[1,4,*]

[1]*Department of Materials Science and Engineering, National Cheng Kung University, Tainan 701, Taiwan*

[2]*Electron Microscopy Center, Empa, Swiss Federal Laboratories for Materials Science & Technology, 8600 Dübendorf, Switzerland*

[3]*Department of Chemical and Materials Engineering, National University of Kaohsiung, Kaohsiung 81148, Taiwan*

[4]*Center for Micro/Nano Science and Technology, National Cheng Kung University, Tainan 701, Taiwan*

(Received 12 August 2011; published 17 October 2011)

The electronic structure of bulk wurtzite ZnO is investigated in valence electron energy loss spectroscopy with scanning transmission electron microscopy. To qualitatively interpret the characteristic spectral feature of ZnO, the complex dielectric function of ZnO is derived from the corresponding low-loss spectra. By scanning the electron probe across the sample from bulk toward the vacuum, four surface excitations intrinsic to ZnO can be identified. The surface plasmon of ZnO appearing around 16 eV is assigned, since with decreasing sample thickness, the volume plasmon is gradually replaced by this spectral feature. Moreover, with the excitation criterion of a negative real part ($\varepsilon_1$) of the dielectric constant of ZnO within this energy regime, the condition for surface plasmon is met. Surface exciton polaritons (SEPs) are found to appear at 9.5 and 13.5 eV, in which the relaxed condition for SEP excitation ($\varepsilon_2 > \varepsilon_1 > 0$) can be fulfilled, with rather weak excitonic oscillator strength (broad interband transitions). In addition, the guided light modes, which are excited by the retardation of incident electrons can be identified at 3.8 eV just above the ZnO bandgap, supported by a calculation employing the Kröger equation.

DOI: 10.1103/PhysRevB.84.155203 PACS number(s): 79.20.Uv, 71.20.Nr

## I. INTRODUCTION

Owing to a direct wide bandgap of about 3.3 eV at 300 K together with a large excitonic binding energy of 60 meV, ZnO has attracted considerable interest and has been applied in a variety of fields such as optical electronics, photovoltaics, chemical sensors, and light emitting diodes.[1–3] To further enhance the functionality of ZnO, a more comprehensive understanding of its fundamental electronic structures is essential. One way of accessing electronic structure information is through the material's dielectric function, which determines the response to external electromagnetic perturbations such as light or electrons. The corresponding optical properties can thus be interpreted and correlated to the electronic structure through their dielectric behavior. Optical quantities of bulk ZnO with a wurtzite structure have been extensively studied by reflection or absorption measurements with light. However, the information thus obtained was mostly limited within the UV spectral range and suffered from poor signal-to-noise ratio, especially in high energy regions. Alternatively, compared to conventional optical methods, the dielectric function extracted from electron energy loss spectroscopy (EELS) in scanning transmission electron microscopy (STEM) can be derived in a much wider frequency range and has excellent spatial resolution, which facilitates probing individual nanoscale materials.[4] As such, also the ZnO optical properties have been investigated by EELS.[5–10] However, the underlying dielectric function has not been applied to explain the spectral features observed in these studies.[5,10] Moreover, the dependence of the energy loss features of ZnO on material size and geometry has been explored by examining nanowires of different sizes under TEM diffraction mode.[7,9] Nevertheless, under such conditions, the obtained results have to be regarded as averaged information, including both surface and volume contributions, which can not genuinely reveal the implicit surface character. Furthermore, the details of the spectral features in the range between 3 eV to 6 eV have rarely been discussed in the literature and thus remain to be resolved.

In this STEM-EELS study, bulk spectra and spectra recorded under aloof beam configuration with a grazing incident electron probe were employed to investigate the electronic properties of ZnO and in particular to distinguish between the surface and volume excitations. Consequently all the surface and volume electronic contributions of ZnO in the low-loss spectrum were successfully identified. Above all, the characteristics of surface-related excitations, including the surface plasmon, surface exciton polaritons (SEPs), and guided light modes are elucidated in detail. Furthermore, spectrum imaging (SI) is introduced to map the spatial distribution of the different electronic excitations.

## II. EXPERIMENTS

Since synthesized ZnO nanostructures suffer from the stoichiometric problems and the strong dependence of crystallinity on fabrication parameters, commercial ZnO powders with well-established composition (Zn:O = 1:1) and microstructure (wurtzite) were thus employed in this study. The ZnO powders were ultrasonically dispersed in anhydrous alcohol and collected on Cu grids with a lacy carbon network followed by subsequent plasma cleaning for removing any contamination. The analysis was performed in STEM mode employing a probe size of about 0.1–0.12 nm, in a probe spherical aberration corrected (Cs-corrected) TEM JEOL 2100F system operated at 200 kV equipped with a Gatan ENFINA spectrometer. The energy resolution was optimized to be 0.6 eV along with the convergence angle of 26 mrad and a collection angle of 14.8 mrad.

## III. RESULTS AND DISCUSSIONS

Figure 1(a)–1(b) shows a series of STEM-EELS spectra acquired with an electron probe scanning across the ZnO

 

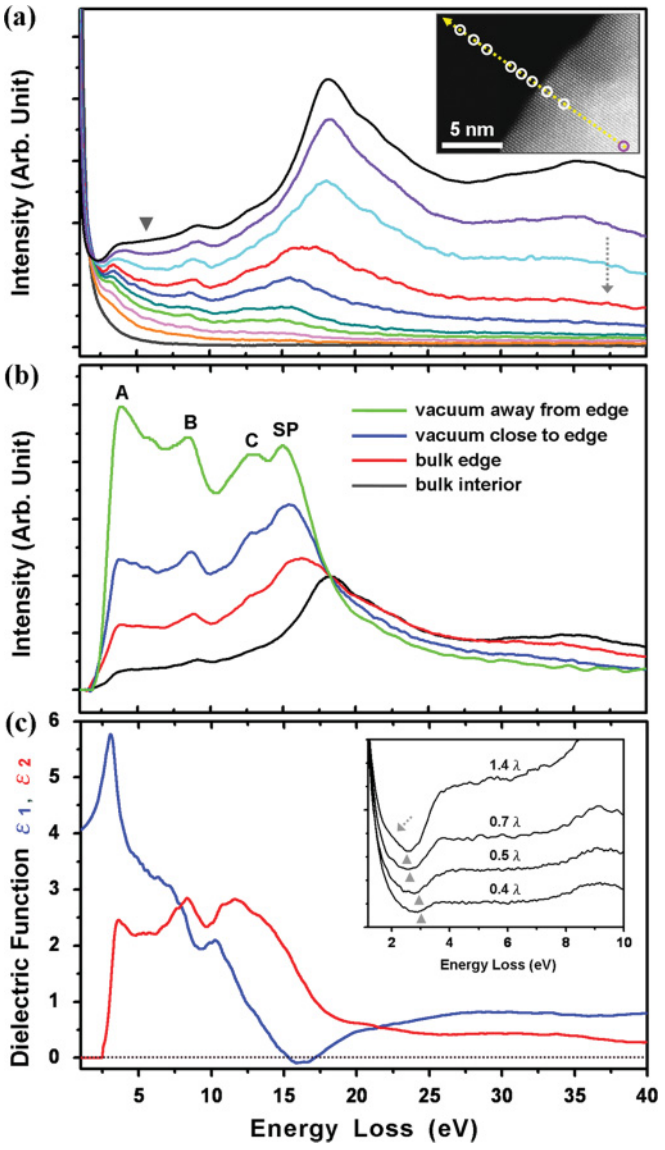


FIG. 1. (Color online) (a) The series of STEM-EELS spectra of ZnO acquired with scanning from the specimen interior to vacuum space, with the circles showing positions in the corresponding HAADF image of ZnO powder (inset). Notice the top black spectrum was obtained from the innermost part of the powder particle (∼1.4 λ). The dashed arrow and the full triangle indicate the scanning direction and thickness-dependent feature at ∼5.5 eV, respectively. (b) Comparison of EELS spectra acquired in the bulk (black), at the edge (red), and with grazing incidence close to (blue) and far from (green) the specimen and vacuum interface normalized to the bulk plasmon intensity at 18.2 eV. (c) Derived complex dielectric function of ZnO ($\varepsilon = \varepsilon_1 + i\,\varepsilon_2$) (inset: variation in spectral feature near the interband transition onset with specimen thickness).

bulk region toward vacuum space. The circles, shown in the high-angle annular dark field (HAADF) image of the ZnO powder [inset of Fig. 1(a)], indicate the positions for spectrum acquisition. The first spectrum [black color in Fig. 1(a), position not shown in the HAADF image] recorded from the innermost part of the sample can be considered to contain the bulk property only, showing corresponding spectral features in the low-loss regime. It consists of a dominant bulk plasmon peak (18.2 eV) together with some broad and relatively weak characteristics at 3.8, 5.5, 9.3, 13.5, 21.8, and 35.5 eV, coinciding with the bulk ZnO electronic structure known from literature.[5,8] Except for the bulk plasmon, these excitations are documented as the interband or intraband transitions from O 2p, 2s, and Zn 3d states in the valence band to the conduction band.[5,8] With locating the probe toward the specimen edge and vacuum, the line shapes of the spectra change in a systemic way [Fig. 1(a)]. Since the inherent physics of the EELS spectra can be understood based on the dielectric response of a medium to the external electromagnetic perturbation, the calculation of frequency or energy-dependent complex dielectric function of ZnO is thus required by performing the Kramers-Kronig analysis (KKA).

For obtaining true electronic structure information from the low-loss spectra, a potential intensity contribution due to retardation radiation should be carefully regarded.[11–13] Retardation effects, such as the generation of Čerenkov radiation (ČR), could extend into the energy region near the bandgap. Hence, such contributions can modify the spectral features resulting in erroneous KKA. However, the emission of ČR is considerably suppressed in thin samples, typically below 100 nm.[14–16] Moreover, as the characteristic scattering angle of the ČR is small (about 0.01 mrad), the effect of ČR can further be reduced if a large collection angle is chosen, such as 14.8 mrad in this study.[13,17] Therefore, even though the relativistic effect can not fully be eliminated, the intensity due to Čerenkov losses can still be kept small under appropriate experimental conditions, which enables reliable dielectric information to be extracted from the low-loss spectra.[17] For various sample thicknesses (0.4–1.4 λ, λ: the inelastic mean free path), the area near the interband transition onset in the EELS spectra has been examined [inset in Fig. 1(c)]. The onset shows a gradual redshift (triangle indexed) with increasing thickness exceeding 0.4 λ along with a change in the shape of the tail of the zero loss peak (ZLP), which is particularly obvious for a thickness of 1.4 λ (dashed arrow). This indicates stronger retardation influence for larger thicknesses. Hence, only the spectra below about 0.5 λ are found to be suitable for a subsequent KKA representative for bulk ZnO. Too thin areas with a high surface to volume ratio should be avoided also, since intense surface excitations may induce inaccuracy in the derivation of the dielectric function as well. Moreover, slabs of ZnO, instead of specific-shaped particles, were preferred to prevent potential shape effects on spectral features. It should be mentioned that the convergence angle of the STEM probe is 26 mrad, which implies that plenty of Bragg-diffracted beams are contributing to the EELS signal. Consequently the anisotropic electronic contributions of wurzite ZnO are averaged out, and each of the spectra along with the corresponding dielectric function in this study can be empirically considered to reflect isotropic behavior.

Figure 1(c) is the complex dielectric function of ZnO derived from the bulk spectrum shown in the Fig. 1(a) of 0.4 λ (purple line). Since the imaginary part $\varepsilon_2$ features a local maximum at the interband transition frequencies,[18] the observed spectral structures at 3.8, 5.5, 9.3, 13.5, 21.8, and 35.5 eV in the low-loss spectrum can thus be properly correlated to the corresponding electronic oscillations within ZnO. The real part of the dielectric constant $\varepsilon_1$ passes through 0 at about 17.1 eV accompanied by a small and decreasing

imaginary part $\varepsilon_2$ ($\varepsilon = 0 + 0.9i$), which corresponds to a maximum for the volume loss function Im $[-1/\varepsilon]$. Hence the excitation appearing as a dominant peak in the loss spectrum can indeed be identified as the volume plasmon of ZnO.[18] The deviation of the observed plasmon position (∼18.2 eV) from the derived frequency $\omega_p$ (17.1 eV) can be interpreted in terms of the interband transitions below $\omega_p$, which shifts the volume plasmon to the higher energy.[18] Moving the electron probe toward the edge of the sample, the bulk plasmon gradually redshifts along with spectral feature broadening [Fig. 1(a)], and it subsequently evolves into another distinct peak at the lower energy side (∼16 eV) with the probe further extending into the vacuum. Accordingly, this spectral feature at ∼16 eV can be designated as the surface plasmon (SP) of ZnO, originating from the collective oscillations of the valence electrons on the surface. The occurrence of SP can further be confirmed by the negative real part $\varepsilon_1$ within this frequency regime (between 15–17 eV). However, this result differs from several recognized values of ZnO SP evaluated by examining ZnO nanowires of different diameters (11.5 eV) [7] or positioning the electron probe along certain polar surfaces (13 eV) [6] with TEM-EELS.

The evanescent wave fields of surface electronic resonances can extend into the vacuum, whereas the volume excitations are relatively localized within the bulk region.[19,20] The aloof geometry, therefore, can thus effectively facilitate the differentiation between surface and volume excitations through the electromagnetic coupling of a grazing electron probe to the evanescent surface eigenmodes. Under this condition the surface spectral features will dominate the low-loss spectra, whereas the volume contributions can be substantially reduced. As a result the SP in the ZnO is clearly determined and discriminated from the volume plasmon. It should be noted that the SP for ZnO can not be appropriately verified with EELS acquisition in the TEM image or diffraction modes, since strong volume excitations in the peripheral region can significantly overwhelm this surface contribution. Furthermore, the spectral variations of the bulk plasmon addressed in the literature, such as an increase in peak width and a redshift with decreasing size down to 20 nm, may not be solely attributed to the proposed increased electron scattering by surface or to the reduction in relaxation time of the oscillations.[7] Instead, they arise from the gradual transition from bulk to surface plasmon with a decrease in the dimensions of the material. Reflection EELS (REELS) measurements with lower incident energy, typically below 900 eV, were used to investigate the surface electronic structure of ZnO film.[22,23] The systematic variation of the intensity between the bulk plasmon and the claimed SP on the probing depth in REELS, seen in these earlier works, agrees with our observation.

Aside from the aforementioned transition of the plasmon excitation when scanning the probe across the sample, the spectral intensities at 5.5, 21.8, and 35.5 eV attenuate drastically, whereas other excitations located at 3.8, 9.3, and 13.5 eV still persist [Fig. 1(a)]. The SP along with the peaks at 3.8, 9.3, and 13.5 eV then become the predominant features, while the electron beam is aloof from the specimen, evidently revealing their surface character. For clarity, a comparison of the EELS spectra acquired in the bulk interior (black), at the edge (red), and with grazing incidence close to (blue) and far from (green) the specimen and vacuum interface is illustrated in Fig. 1(b). Please notice that the spectra are deconvoluted with the removal of ZLP and then normalized according to the intensity of the bulk plasmon. This normalization thus enhances the relative intensity of the surface contributions (green and blue curves). Clearly distinct variations in their line shapes can be observed, and it's interesting to elucidate the rarely addressed surface electronic resonances occurring at 3.8 (*A*), 9.3 (*B*), and 13.5 (*C*) eV in Fig. 1(b).

Recently the fundamental physics of SEPs has been reconsidered and experimentally investigated by EELS.[21–23] The SEPs are collective surface electromagnetic waves attenuating along the boundaries, which results from the strong coupling of the external electromagnetic field with the delocalized excitons at the surface of the medium. The existence of SEPs requires the materials to show strong excitonic absorption, where the imaginary part ($\varepsilon_2$) of the corresponding complex dielectric function ($\varepsilon = \varepsilon_1 + i\,\varepsilon_2$) is much greater than the real part ($\varepsilon_1$): $\varepsilon_2 \gg \varepsilon_1 \geqq 0$, revealing as a sharp peak in $\varepsilon_2$.[24–26] However, Chu *et al*. have demonstrated the relaxed criterion for SEP excitation even with $\varepsilon_2 > \varepsilon_1 > 0$,[21] which can then be found in many materials such as semiconductors or insulators above bandgaps and metals in the insulating spectral regime. The existence of SEPs in metallic Au nanoparticles,[21] $HfO_2$[22], and GaN[23] has also been experimentally confirmed.

Through a detailed examination of the derived dielectric function of ZnO [Fig. 1(c)], distinct excitonic absorptions in the imaginary part of dielectric function ($\varepsilon_2$) can be observed at 8.2 eV and between 10.6 eV to 13.4 eV. Accordingly the spectral shoulder (9.3 eV) along with a broader hump (13.5 eV) nearby, shown in the low-loss spectra recorded in bulk interior [black line in Fig. 1(a)], can thus be regarded as the result of interband transitions. Given that the SEP excitation of $\varepsilon_2 > \varepsilon_1 > 0$ within the above-mentioned energy regime is satisfied, the excitonic oscillators could result in collective resonance of delocalized excitons on the surface of the material. Therefore, the excitations of surface nature revealed as a distinct peak *B* (9.3 eV) and a broader hump *C* (centered at 13.5 eV) for grazing incidence [see green spectrum in Fig. 1(b)], can be assigned to reflect the contributions from SEP eigenmodes according to the criterion $\varepsilon_2 > \varepsilon_1 > 0$.

For loss spectra acquired under TEM image or diffraction modes, the SEP features, although intrinsic to ZnO, can significantly be buried by the dominant contribution of interband transition (8.2–13.4 eV). Contrarily, with the assistance of a spatially resolved aloof STEM probe, the volume electronic contributions are strongly suppressed, and the SEPs can thus be clearly resolved. It is worthy to mention that the observed peak *C* of SEP origin can not be properly interpreted according to the dielectric function of ZnO derived from EELS in the literature,[10] where the intensity of $\varepsilon_2$ is below $\varepsilon_1$ ($\varepsilon_2 < \varepsilon_1$) in an energy range of 7–10 eV. The accuracy of our presented relative intensities between $\varepsilon_1$ and $\varepsilon_2$ ($\varepsilon_2 > \varepsilon_1$) in this frequency regime can be further supported by a recent report on ZnO optical properties analyzed with synchrotron radiation.[27]

With regard to the remaining spectral feature peak *A*, it could probably arise from the guided light mode, which is related to the retardation radiation effects, involving collective excitations of electrons inside the medium. In this condition, from the optical point of view, two waves of total internal

reflection can be envisaged to travel back and forth between the boundaries of the bulk. The resultant superposed wave then propagates along the surface with a standing wave field built across the boundary of the film that evanescently decays into the vacuum. The guided light modes have their maximum or maxima within the material, which is in distinct contrast to the nonradiative SP with their strongest amplitude at the boundaries.[18] To excite the guided waves, the real part ($\varepsilon_1$) of the dielectric constant of medium must be greater than 1 together with a small imaginary part $\varepsilon_2$.[18] The incident electron beam could additionally undergo another loss caused by ČR.[11,18] While swift electrons penetrate a thin foil, atoms in the bulk can be polarized by the external electromagnetic perturbation and virtual photons are promptly emitted after restoring to the equilibrium. Provided the semi-relativistic electrons travel exceeding the phase velocity of light propagating inside the dielectrics, $c/\sqrt{\varepsilon_1}$ ($c$ the speed of light in vacuum and $\varepsilon_1$ the real part of dielectric constant of medium), a coherent and constructive photonic wave front can be built along the trajectory of electrons, further leading to energy loss of the incident beam. This radiation associated with relativistic retardation is designated as ČR and is particularly essential for the substances with high dielectric constants within a certain frequency region. However, the size of the photonic wave front limits this effect to thicker samples.

Looking at the dielectric function in Fig. 1(c), the guided mode can be excited below about 3.8 eV. Furthermore the emission of ČR could be feasible below 9 eV, in which $\varepsilon_1 > 2$, leading to the electron velocity (about $0.7c$ for 200 keV electrons here) beyond the finite speed of light in ZnO. For a ZnO slab in vacuum and 200-keV electrons, the characteristic angle of ČR cone is about 50° (3.8-eV radiation), which is larger than the threshold (30°) for total internal reflection in the ZnO and vacuum interface. The emitted light thus cannot escape and then is confined within the medium. Therefore, the energy-loss feature at 3.8 eV above bandgap onset can be attributed to the excitation of guided light modes coupled to the confined ČR (i.e., guided Čerenkov modes), associated with the retardation of incident electrons inside the dielectric medium.[15,28]

Moreover it is also worthwhile to specify another thickness-dependent spectral feature located around 5.5 eV. Figure 2 shows the comparison between the loss spectra obtained within the bulk interior of different thicknesses. It can be found that the spectral feature at 5.5 eV appears as a broad shoulder just above peak $A$ for the relatively thicker regions above 1.0 λ, whereas its intensity decreases gradually for thinner areas of 0.3–0.5 λ (dashed arrow in Fig. 2). This variation is also well revealed in the line scanning result (between black and purple spectra in Fig. 1(a), as indicated by the triangle). To better understand the physical origin of this characteristic, the Kröger equation,[29] which describes all relevevant low-loss spectral features of a thin slab including bulk, surface, and retardation effects, is thus introduced.

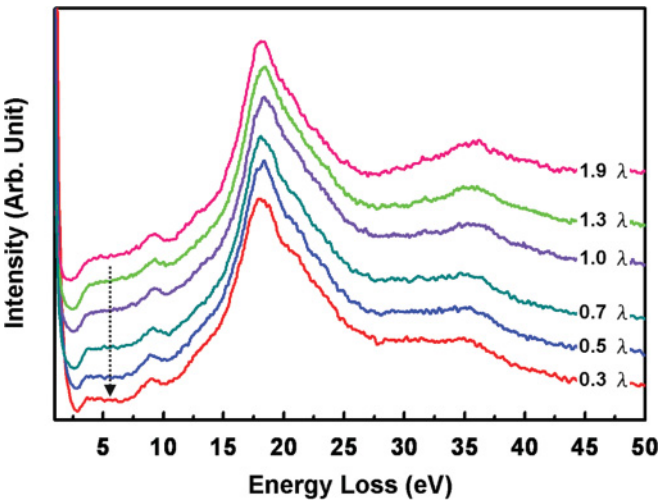


FIG. 2. (Color online) Comparison between the EELS spectra acquired for different specimen thicknesses (λ: the inelastic mean free path). The systematic variation of the thickness-dependent spectra shoulder at ~5.5 eV is marked by a dashed arrow.

Maps of the energy-loss probability, calculated with the Kröger equation according to the extracted ZnO dielectric function [Fig. 1(c)], are presented in $E$–$\theta$ planes ($E$: energy loss and $\theta$: scattering angle of incident electrons) for two different slab thicknesses of 240 and 60 nm (Fig. 3), which approximately reflect the thickness of the spectra acquired at 1.9 and 0.5 λ, respectively. For our experiment parameters,

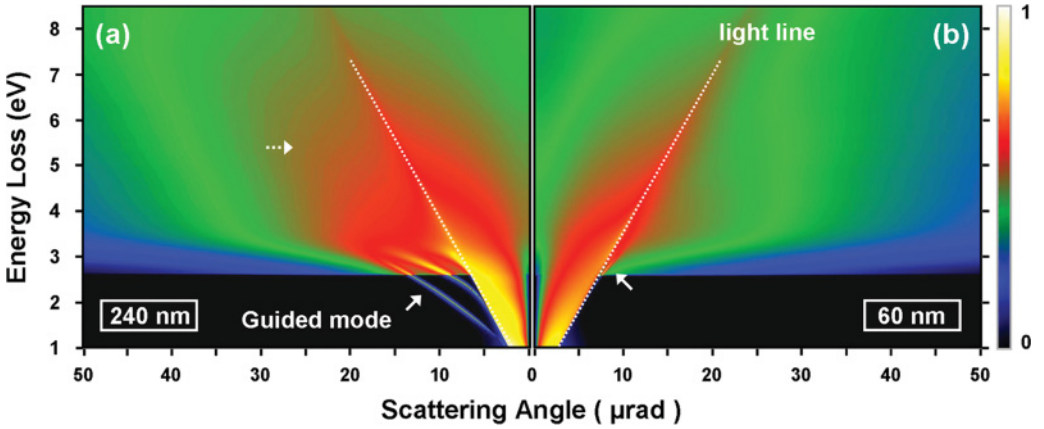


FIG. 3. (Color online) Log-scaled simulated relativistic loss probabilities in the $E$–$\theta$ maps ($E$: energy loss and $\theta$: scattering angle of incident electrons) for ZnO slab thicknesses of (a) 240 nm and (b) 60 nm, according to the derived dielectric function in Fig. 1(c). Solid and dashed arrows indicate the guided light modes and their extension of dispersive curve to the energy regime of 3.8–5.5 eV, respectively.

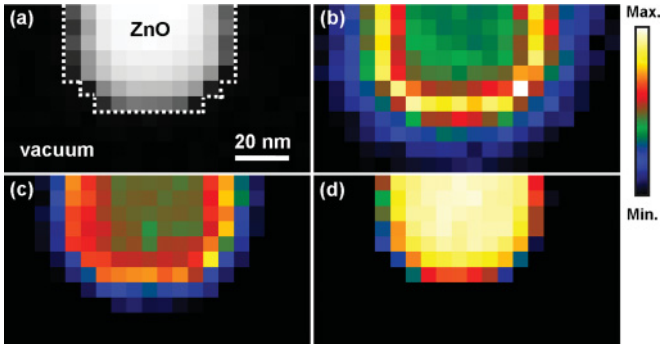


FIG. 4. (Color online) SI mapping for the different excitations: (a) raw SI image with dashed line showing the boundary of ZnO powder, (b) guided light modes (3.8 eV), (c) SEPs (5.5 eV), and (d) bulk plasmon (18.2 eV).

the inelastic mean free path $\lambda$ of ZnO is estimated to be about 122 nm from the formalism in Ref. 30. To correlate to the obtained data, it should be pointed out that the experimental EELS spectra reflect the angular integration of all loss probability over the scattering angle range defined by the effective collection angle. For the slab of 240 nm, the $E$–$\theta$ map reveals three guided light modes with their characteristic dispersion [solid arrow in Fig. 3(a)], while only one guided branch close to light line can be distinguished for the 60-nm slab [Fig. 3(b)]. This result further supports the identification of peak $A$ with the guided wave nature. With reduction in thickness, low-energy modes disappear since the corresponding longer wavelength cannot be confined in a thin slab anymore [Fig. 3(b)]. For thickness less than 50 nm ($\sim$0.4 $\lambda$), the $E$–$\theta$ maps (not shown) reveal rather weak retardation features below the interband transition onset, certifying its reliability for KKA. Examining the simulated $E$–$\theta$ maps for the 240-nm slab, the apparent guided dispersive curves further extend into the energy region between 3.8 and 5.5 eV [(Fig. 3(a)], dashed arrow). Therefore, the pronounced spectral shoulder above peak $A$, shown in the spectra acquired at thicker areas possibly stems from the integration of contributions due to the guided light modes. This feature weakens with decreasing thickness where guided light modes become less probable. Some ZnO low-loss spectra in the literature bearing the above-mentioned feature obviously,[31] indicating the rather thick specimens employed.

The SI results in Fig. 4 illustrate the spatial distribution maps for the corresponding excitations of the guided light modes (3.8 eV), the SEPs (5.5 eV), and the bulk plasmon (18.2 eV). The scanning step for each pixel is about 4 nm. The map of the surface modes can extend further into the vacuum and reveals rather intense signals at bulk and vacuum boundaries, as expected for nonradiative surface electromagnetic waves [Figs. 4(b) and 4(c)], whereas the intensity of the volume plasmon is strongly localized within the bulk interior [Fig. 4(d)]. Moreover, for the guided modes and SEPs, the variation in decaying distances of wave field to free space can be interpreted in terms of the decay constant, which is proportional to $\omega/\upsilon$ ($\omega$: the frequency of surface excitation and $\upsilon$: the incident electron velocity),[19,21] indicating greater persistence for lower energy modes.

## IV. CONCLUSION

In conclusion, the electronic structure of wurtzite ZnO has been studied by discussing the spectral features and the dielectric function derived from STEM-EELS experiments. The excitations of volume nature and the appearance of surface-driven modes in thin specimen area have been involved in detail. Three types of surface eigenmodes have been specified in this material system. The presence of a surface plasmon at $\sim$16 eV is confirmed, which is in agreement with the negative real part $\varepsilon_1$ within this spectral regime (about 15–17 eV). The existence of two SEP modes at $\sim$9.5 and $\sim$13.5 has been established under the relaxed SEP-excitation condition of $\varepsilon_2 > \varepsilon_1 > 0$, in which weak excitonic absorptions in the peripheral region can be found. Furthermore, the guided light modes coupled to the confined ČR at about 3.8 eV above ZnO bandgap onset can also be identified.

## ACKNOWLEDGMENTS

The authors would like to convey the most sincere appreciation to Professor Yung-Chiang Lan in the Institute of Electro-Optical Science and Engineering in NCKU for fruitful and constructive discussion in plasmon physics. This work was also financially supported by the National Science Council of Taiwan (Research Grant NSC-98-2221-E-006-079-MY3).

*cpliu@mail.ncku.edu.tw

[1] R. C. Wang, C. P. Liu, J. L. Huang, and S. J. Chen, Nanotechnology **17**, 753 (2006).
[2] C. L. Kuo, R. C. Wang, J. L. Huang, C. P. Liu, Y. F. Lai, C. Y. Wang, and H. C. Chung, Nanotechnology **19**, 285703 (2008).
[3] R. C. Wang and H. Y. Lin, Sens. Actuators B Chem. **149**, 94 (2010).
[4] R. Erni and N. D. Browning, Ultramicroscopy **104**, 176 (2005).
[5] R. L. Hengehold, R. J. Almassy, and F. L. Pedrotti, Phys. Rev. B **1**, 4784 (1970).
[6] Y. Ding and Z. L. Wang, J. Electron Microsc. **54**, 287 (2005).
[7] J. Wang, X. P. An, Q. Li, and R. F. Egerton, Appl. Phys. Lett. **86**, 201911 (2005).
[8] Z. H. Zhang, X. Y. Qi, J. K. Han, and X. F. Duan, Micron **37**, 229 (2006).
[9] J. Wang, Q. Li, and R. F. Egerton, Micron **38**, 346 (2007).
[10] Z. H. Zhang, M. He, and Q. Li, Solid State Commun. **149**, 1856 (2009).
[11] M. Stoger-Pollach and P. Schattschneider, Ultramicroscopy **107**, 1178 (2007).
[12] M. Stoger-Pollach and T. Galek, Micron **37**, 748 (2006).

[13]M. Stoger-Pollach, H. Franco, P. Schattschneider, S. Lazar, B. Schaffer, W. Grogger, and H. W. Zandbergen, Micron **37**, 396 (2006).
[14]C. Vonfeste, Z. Phys. **227**, 453 (1969).
[15]C. H. Chen, J. Silcox, and R. Vincent, Phys. Rev. B **12**, 64 (1975).
[16]R. Erni and N. D. Browning, Ultramicroscopy **108**, 84 (2008).
[17]L. Gu, V. Srot, W. Sigle, C. Koch, P. van Aken, F. Scholz, S. B. Thapa, C. Kirchner, M. Jetter, and M. Rühle, Phys. Rev. B **75**, 195214 (2007).
[18]H. Raether, *Excitations of Plasmons and Interband Transitions by Electrons* (Springer-Verlag, Berlin, 1980).
[19]F. J. Garcia de Abajo and A. Howie, Phys. Rev. B **65**, 115418 (2002).
[20]M. W. Chu, V. Myroshnychenko, C. H. Chen, J. P. Deng, C. Y. Mou, and F. J. G. de Abajo, Nano Lett. **9**, 399 (2009).
[21]M. W. Chu, C. H. Chen, F. J. Garcia de Abajo, J. P. Deng, and C. Y. Mou, Phys. Rev. B **77**, 245402 (2008).
[22]S. C. Liou, M. W. Chu, Y. J. Lee, M. Hong, J. Kwo, and C. H. Chen, New J. Phys. **11**, 103009 (2009).
[23]C. T. Wu, M. W. Chu, L. C. Chen, K. H. Chen, C. W. Chen, and C. H. Chen, Micron **41**, 827 (2010).
[24]F. Yang, J. R. Sambles, and G. W. Bradberry, Phys. Rev. Lett. **64**, 559 (1990).
[25]F. Z. Yang, J. R. Sambles, and G. W. Bradberry, Phys. Rev. B **44**, 5855 (1991).
[26]F. Z. Yang, G. W. Bradberry, and J. R. Sambles, Phys. Rev. Lett. **66**, 2030 (1991).
[27]P. Gori, M. Rakel, C. Cobet, W. Richter, N. Esser, A. Hoffmann, R. Del Sole, A. Cricenti, and O. Pulci, Phys. Rev. B **81**, 125207 (2010).
[28]A. Yurtsever, M. Couillard, and D. A. Muller, Phys. Rev. Lett. **100**, 217402 (2008).
[29]E. Kröger, Z. Phys. **216**, 115 (1968).
[30]T. Malis, S. C. Cheng, and R. F. Egerton, J. Electron Microsc. Tech. **8**, 193 (1988).
[31]K. Jarausch, P. Thomas, D. N. Leonard, R. Twesten, and C. R. Booth, Ultramicroscopy **109**, 326 (2009).